Laser and Particle Beams (2016), *34*, 545–551.
© Cambridge University Press, 2016 0263-0346/16
doi:10.1017/S0263034616000446

Effect of transverse magnetic fields on high-harmonic generation in intense laser–solid interaction

J. MU,[1] F.-Y. LI,[2] Z.-M. SHENG,[1,2] AND J. ZHANG[1]

[1]Key Laboratory for Laser Plasmas (MoE) and Department of Physics and Astronomy, Shanghai Jiao Tong University, Shanghai 200240, China

[2]SUPA, Department of Physics, University of Strathclyde, Glasgow G4 0NG, UK

(Received 18 April 2016; Accepted 20 June 2016)

Abstract

The effect of transverse magnetic fields on surface high-harmonic generation in intense laser–solid interactions is investigated. It is shown that the longitudinal motion of electrons can be coupled with the transverse motion via the magnetic fields, which lead to even-order harmonics under normal laser incidence. The dependence of the coupling efficiency and hence even harmonic generation with preplasma scale length and magnetic field strength are presented based upon particle-in-cell simulations. When the magnetic field is parallel to the laser electric field, the spectral intensity of the second harmonic is proportional to the magnetic field strength in a wide range up to 160 MG, while the situation with the magnetic field perpendicular to the laser electric field is more complicated. The second harmonic generation due to the magnetic field also tends to increase with the plasma density scale lengths, which is different from the high-harmonic generation by the oscillating mirror mechanism. With the increase of the laser spot size from a laser wavelength λ_L, both the magnetic field-induced harmonics and oscillating mirror high harmonics tend to increase first and then become saturated after $3\lambda_L$. The magnetic field-induced second harmonic may be used to evaluate large self-generated magnetic fields developed near the critical density region and the preplasma conditions.

Keywords: High-harmonic generation; Laser–plasma interaction; Magnetic field

1. INTRODUCTION

High-harmonic generation in intense short-pulse laser interaction with solid targets contains rich information of the instantaneous dynamics that are deeply rooted in the highly nonlinear process. It thus has led to diverse applications such as measuring the hole-boring speed for fast ignition researches (Zepf *et al*., 1996; Weng *et al*., 2015) and sensing megagauss (MG) magnetic fields in solids heated by intense lasers (Tatarakis *et al*., 2002). Another major application is to produce extremely short light pulses down to attoseconds (Földes *et al*., 2003; Mairesse *et al*., 2003). Solid surface harmonics can provide intense enough attosecond pulses for probing ultrafast dynamics within the atomic timescale (Tsakiris *et al*., 2006). Polarization gating is used as a control of surface oscillations of solid targets to produce isolate attosecond pulses (Yeung *et al*., 2015).

Address correspondence and reprint requests to: Z.-M. Sheng, Key Laboratory for Laser Plasmas (MoE) and Department of Physics and Astronomy, Shanghai Jiao Tong University, Shanghai 200240, China and SUPA, Department of Physics, University of Strathclyde, Glasgow G4 0NG, UK. E-mail: zmsheng@sjtu.edu.cn

In surface high-harmonic generation (SHHG), an intense laser pulse is reflected by relativistically oscillating layers of surface electrons driven by the laser pulse itself (Bulanov *et al*., 1994; Lichters *et al*., 1996). Under normal incidence, the reflected pulses contain only odd harmonics polarized in parallel to the drive pulse, which have been modeled using a sharp vacuum–plasma interface and follows the well-known selection rules (Lichters *et al*., 1996). In practice, additional conditions will also contribute, the first being preplasma expansion attributed to electron preheating arising from either the rising edge of incident pulses, prepulses, or a second pulse sent prior to the main pulse (Macphee *et al*., 2010; Ma *et al*., 2012). The efficiency of SHHG was found to be sensitive to the preplasma scale length (Ozaki *et al*., 2007), dramatically enhanced in certain range because of a lower density involved and deteriorated again for longer expansion (Dollar *et al*., 2013; Kahaly *et al*., 2013). The density gradient also plays a key role in the harmonic generation mechanism of coherent wake emission (Sheng *et al*., 2005; Quéré *et al*., 2006). The fine control of preplasma expansion has become a critical step toward efficient SHHG.

https://doi.org/10.1017/S0263034616000446 Published online by Cambridge University Press

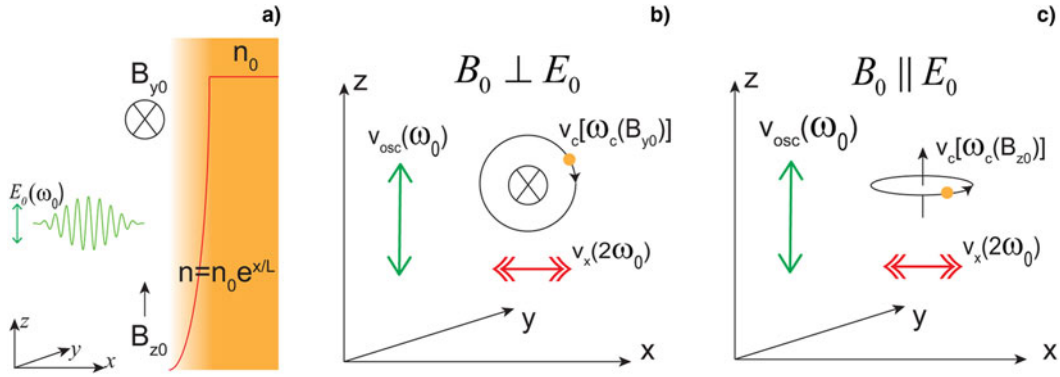


Fig. 1. (a) Sketch of the interaction configuration with the incident laser along the x-direction and polarized along the z-direction. (b, c) illustrate electron motion near the target surface under the interaction of incident laser and the transverse magnetic field either perpendicular or parallel to the laser electric field, respectively.

Additional complexity of SHHG may also come from self-generated magnetic fields. Quasi-static magnetic fields of 100 MG are shown to exist in the near-critical density region of solids via laser ponderomotive heating (Sudan, 1993; Mason & Tabak, 1998) as well as fast electron current. Typically these fields are along the azimuthal direction for laser normal incidence and are important to a number of processes such as laser absorption, laser-driven ion acceleration, and fast electron transport (Stambulchik *et al.*, 2007). Potentially, such quasi-static magnetic fields can also affect SHHG, which has not been clarified completely. In magnetized plasmas, the conversion of a fraction of a laser beam to its phase-mismatch second and third harmonics was analyzed with single-particle model (Ghorbanalilu, 2012). It was also suggested that the coupling between the laser-driven oscillations and electron cyclotron motion in such magnetic fields can generate sidebands in the vicinity of harmonics (Zheng *et al.*, 2002).

In this paper, we explore the effect of high transverse magnetic fields on SHHG using particle-in-cell (PIC) simulations. The full process should incorporate target expansion and magnetic field generation due to pre-heating in picoseconds and subsequent high-harmonic generation through femtosecond main pulse interactions. Here, we simplify the treatment by combining a clean femtosecond drive pulse, an external magnetic field of over 10 MG transverse to the laser direction and a pre-defined preplasma region. This can be used to mimic some conditions of relativistic laser–solid interaction under which high quasi-static magnetic fields at tens of MG might exist, even though such high fields are currently not possible in laboratory with conventional technologies. As we shall see, the presence of transverse magnetic fields alters appreciably the electron dynamics near the target surface due to the cyclotron motion. Coupling with surface longitudinal oscillations, they lead to even-order harmonics for simple normal-incidence geometry. In particular, when the magnetic field is parallel to the direction of the laser electric field, the intensity of these even harmonics shows well-behaved dependence with the magnitude of the exerted magnetic field strength, readily observable in experiments. Thus, these results may not only allow the dynamic evolution of self-generated magnetic fields in the relativistic laser–solid interaction to be diagnosed via a pump–probe scheme, but also provide an active monitoring of surface dynamics by exerting a transverse magnetic field even if just at a few Tesla.

2. THEORY MODEL

Qualitatively, the effect of a transverse magnetic field on the surface motion of electrons and subsequent SHHG can be sketched with Figure 1. Assume a linearly polarized short intense laser pulse propagates along x-direction and normally irradiates onto a foil target, which is placed under a uniform transverse magnetic field $\boldsymbol{B}_0 = B_{0y}\hat{y} + B_{0z}\hat{z}$, as shown in Figure 1a. It is well known that electrons under the laser interaction will experience transverse oscillation along the laser electric field along the z-direction at the laser frequency ω_0 and the longitudinal oscillation along the x-direction at $2\omega_0$, which form the xz-plane. The coupling of longitudinal and transverse oscillations only leads to odd harmonics with the same polarization of the driving laser. When there is a transverse magnetic field B_0, these oscillations will couple with the cyclotron motion. In the case when this magnetic field is perpendicular to the laser electric field as shown in Figure 1b, the cyclotron motion will be within the xz-plane. Therefore a new surface current component along the z-direction at $2\omega_0$ will appear. As a result, both odd and even harmonics will be produced with the same polarization of the driving laser, which is different from the case without the magnetic field. On the other hand, when this magnetic field is parallel to the laser electric field as shown in Figure 1c, the cyclotron motion will be in a plane perpendicular to the xz-plane. Therefore a new surface current component along the y-direction at $2\omega_0$ will appear. As a result, even harmonics polarized long the y-direction will be produced, while only odd harmonics with the same polarization of the driving laser.

Mathematically, the above scenario can be described by the equation of electron motion coupled with the Maxwell's

https://doi.org/10.1017/S0263034616000446 Published online by Cambridge University Press

equations. Under both the laser and magnetic fields, the equation of motion reads

$$\frac{d\boldsymbol{p}}{dt} = -e[\boldsymbol{E} + \boldsymbol{v} \times (\mathbf{B} + \boldsymbol{B}_0)], \tag{1}$$

where $\boldsymbol{p}$, $\boldsymbol{v}$, and $-e$ are, respectively, the electron momentum, velocity, and charge of electrons, $\mathbf{E} = -\partial\mathbf{A}/\partial t - \nabla\phi$, $\mathbf{B} = \nabla \times \mathbf{A}$, ϕ is the electrostatic potential and $\mathrm{a} = \mathrm{e}\mathbf{A}/m_e c$ is the normalized laser vector potential with m_e and c being the electron mass and light speed in the vacuum. By combining Eq. (1) and the Maxwell's equations, the polarized vector potentials a_y (p-polarized) and a_z (s-polarized) satisfy the following wave equations:

$$\begin{aligned}(\partial_x^2 - \frac{1}{c^2}\partial_t^2)\mathrm{a}_y &= \left(\frac{\omega_\mathrm{p}}{c}\right)^2 s_y,\\ (\partial_x^2 - \frac{1}{c^2}\partial_t^2)\mathrm{a}_z &= \left(\frac{\omega_\mathrm{p}}{c}\right)^2 s_z\end{aligned} \tag{2}$$

with the source terms

$$\begin{aligned}s_y &= n\sqrt{1-\beta_x^2}\,\frac{a_y'}{\sqrt{1+a_y'^2+a_z'^2}},\\ s_z &= n\sqrt{1-\beta_x^2}\,\frac{a_z'}{\sqrt{1+a_y'^2+a_z'^2}}.\end{aligned} \tag{3}$$

Here $a_y' = a_y + eB_{0z}/m\int_t \beta_x dt$ and $a_z' = a_z - eB_{0y}/m\int_t \beta_x dt$ with β_x being the longitudinal electron velocity normalized by c, $\omega_\mathrm{p} = \sqrt{n_0 e^2/m\varepsilon_0}$ is the plasma frequency defined by the maximum initial electron density n_0, n is the electron density normalized by n_0, and ε_0 is the vacuum permittivity.

The above equations reduce to that derived in (Lichters *et al.*, 1996) for $B_{0y} = B_{0z} = 0$. For example, for an s-polarized drive laser pulse, both the density fluctuation n and longitudinal velocity β_x contain only even-order harmonics of the laser frequency ω_L. Coupling with transverse laser oscillations, they lead to only odd harmonics polarized in the same plane as the drive pulse. While for nonzero B_0, the presence of the magnetic field modifies the vector potentials in the source terms with an additional terms $eB_{0z}/m\int_t \beta_x dt$ and $-eB_{0y}/m\int_t \beta_x dt$. Obviously, the additional terms are due to the cyclotron motion exerted by the magnetic field and the surface longitudinal oscillations β_x. In particular, additional even harmonics polarized orthogonal to the magnetic field, apart from the typical odd harmonics polarized in parallel to the drive pulse. Despite this simple qualitative analysis, the dependence of the even harmonic generation with laser–target and magnetic field parameters are quite complicated as the cyclotron motion and longitudinal oscillation are strongly coupled with each other. The cyclotron motion spreads over the entire region, while density oscillation is most efficient only near the critical density surface. Under sufficient strong magnetic field, the cyclotron motion can also modify the surface oscillations. In the following, we adopt PIC simulations to elucidate the details and provide parametric studies of this phenomenon.

3. NUMERICAL SIMULATION RESULTS

3.1. One-dimensional (1D) PIC simulation

We start with 1D PIC simulations using the OSIRIS code (Fonseca *et al.*, 2002). The simulation box is initialized as $40\lambda_\mathrm{L}$ long, divided into 4000 cells with 100 micro-particles per cell, where λ_L is the incident laser wavelength. The solid target is uniform in $x \in [0, 2\lambda_\mathrm{L}]$, with a preplasma attached in the front varying as $n = n_0 \exp(x/L)$, where $n_0 = 40\, n_\mathrm{c}$ is the peak density, $n_\mathrm{c} = 1.1 \times 10^{21}\ \mathrm{cm}^{-3}$ is the critical density for $\lambda_\mathrm{L} = 1\ \mu\mathrm{m}$, and $L = 0.2$ is the preplasma scale length. A linearly polarized laser pulse with normalized vector potential $a = a_0 \sin^2(\pi t/T_\mathrm{L})$ impinges from the left onto the target, where $a_0 = 0.5$ corresponds to a peak intensity of $3.4 \times 10^{17}\ \mathrm{W/cm^2}$, $\tau = 9T_\mathrm{L}$ is the full pulse duration, and $T_\mathrm{L} = 2\pi/\omega_0$ is the laser period. For clarity, we assume it is polarized along the z-direction and call it s-polarized. Ions are treated to be stationary background as they have little effect in this ultrafast process (An der Brügge *et al.*, 2012).

The reflected pulses are traced at $x = -4$ and the results (both time and frequency domains) are shown in Figure 2 for different runs with or without external magnetic field in different directions. In the case without external magnetic field, only odd harmonics show up in s-polarization and no harmonics is observed in p-polarization, as shown by the

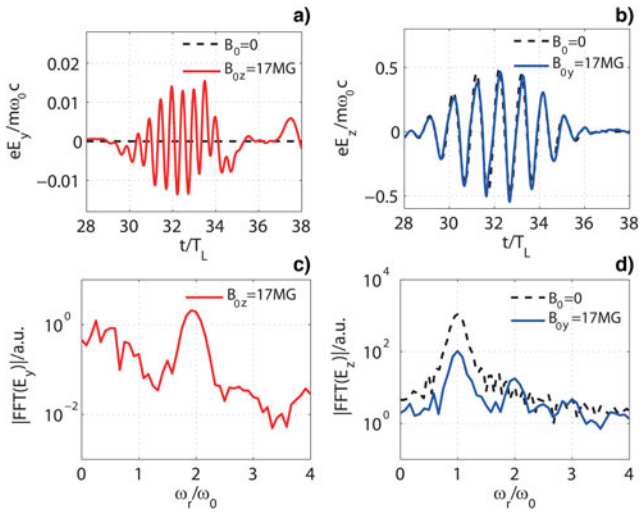


Fig. 2. An s-polarized laser pulse is reflected by a solid target in different runs without and with a homogeneous magnetic field applied either in y- or z-directions. The p- and s-polarized components of the reflected electric field without the effect of magnetic field are plotted in black dashed lines in (a) and (b). The p-polarized component of the reflected electric field E_y in $B_{0z} = 17$ MG and its Fourier transformed spectra are shown in red solid lines in (a) and (c). The s-polarized component of the reflected electric field E_z in $B_{0y} = 17$ MG and its Fourier transformed spectra are shown in blue solid lines in (b) and (d).

https://doi.org/10.1017/S0263034616000446 Published online by Cambridge University Press

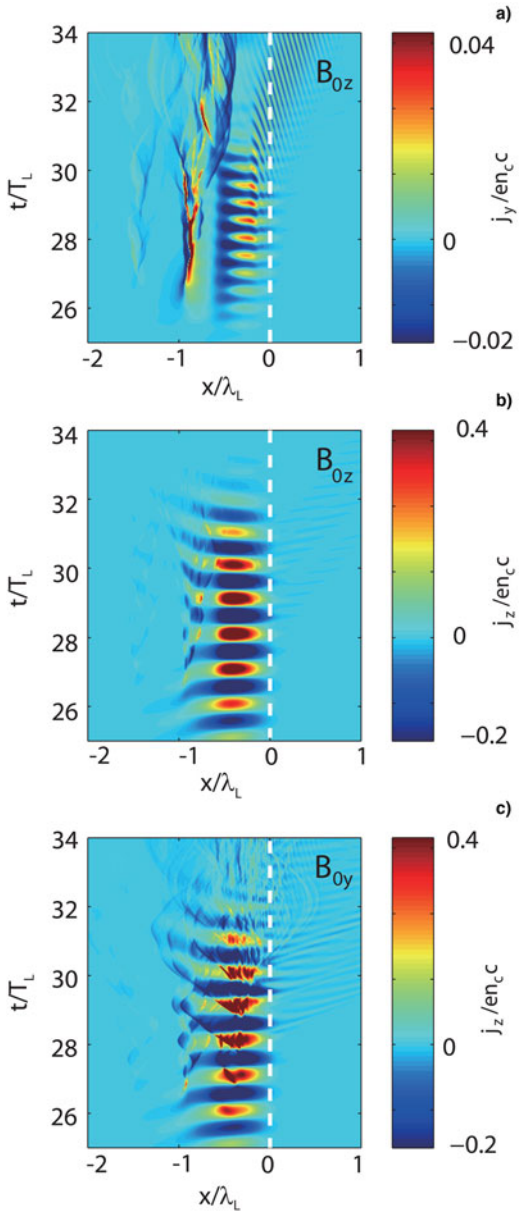


Fig. 3. Space-time plots of electric current components j_y and j_z vs coordinate x and time t in units of λ_L and T_L with a magnetic field applied either in z- or y-directions. (a, b) are for j_y and j_z respectively with $B_{0z} = 17$ MG, and (c) is for j_z with $B_{0y} = 17$ MG. The dashed line shows the initial position of the critical plasma density.

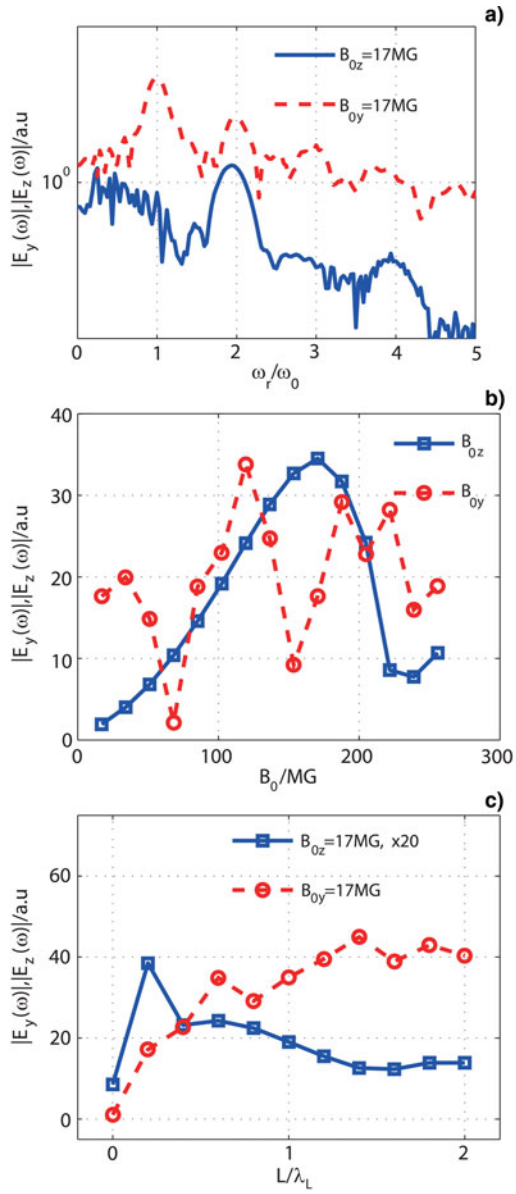


Fig. 4. (a) The Fourier transformed spectra of E_y with the magnetic field $B_{0z} = 17$ MG (blue solid) and E_z with $B_{0y} = 17$ MG (red dashed) with $L = 0.2\ \lambda_L$. (b) Scalings of the second-harmonic spectra |FFT(E_y)| (blue square) and |FFT(E_z)| (red circle) with the strength of the magnetic field B_{0z} and B_{0y}, respectively, with $L = 0.2\ \lambda_L$. (c) Scalings of the second-harmonic spectra |FFT(E_z)| (red circle) either with $B_{0y} = 17$ MG and |FFT(E_y)| (blue square, multiplied by 20) or with $B_{0z} = 17$ MG with the preplasma length.

black dashed lines in Figure 2a, 2b, 2d, as expected in accordance with the selection rules (Lichters *et al.*, 1996). The prominent new feature occurs for $B_{0z} = 17$ MG, where a well-defined reflected pulse containing even-order laser harmonics now emerges in p-polarization as shown in Figure 2c. The even-order harmonics occur in s-polarization for $B_{0y} = 17$ MG, as shown in Figure 2d. The parity of these even harmonics changes with the direction of the external magnetic field and they are always perpendicular to the magnetic field, a clear evidence of electron cyclotron motion as theoretically discussed above. The merit of employing parallel magnetic field and incident laser field is that the even harmonics can be well separated from the reflection of the drive pulse due to their different polarizations.

The harmonics generation due to the magnetic field is also reflected in the transverse currents, which are actually the source terms give in Eq. (2). In Figure 3, the electric current components j_y and j_z in different simulations run with the transverse magnetic field either perpendicular or parallel to the laser electric field are shown in the space-time plots. With the presence of magnetic field $B_{0z} = 17$ MG, a new surface current j_y at $2\omega_0$ appears as shown in Figure 3a, resulting in the even harmonics in |FFT(E_y)| shown in

https://doi.org/10.1017/S0263034616000446 Published online by Cambridge University Press

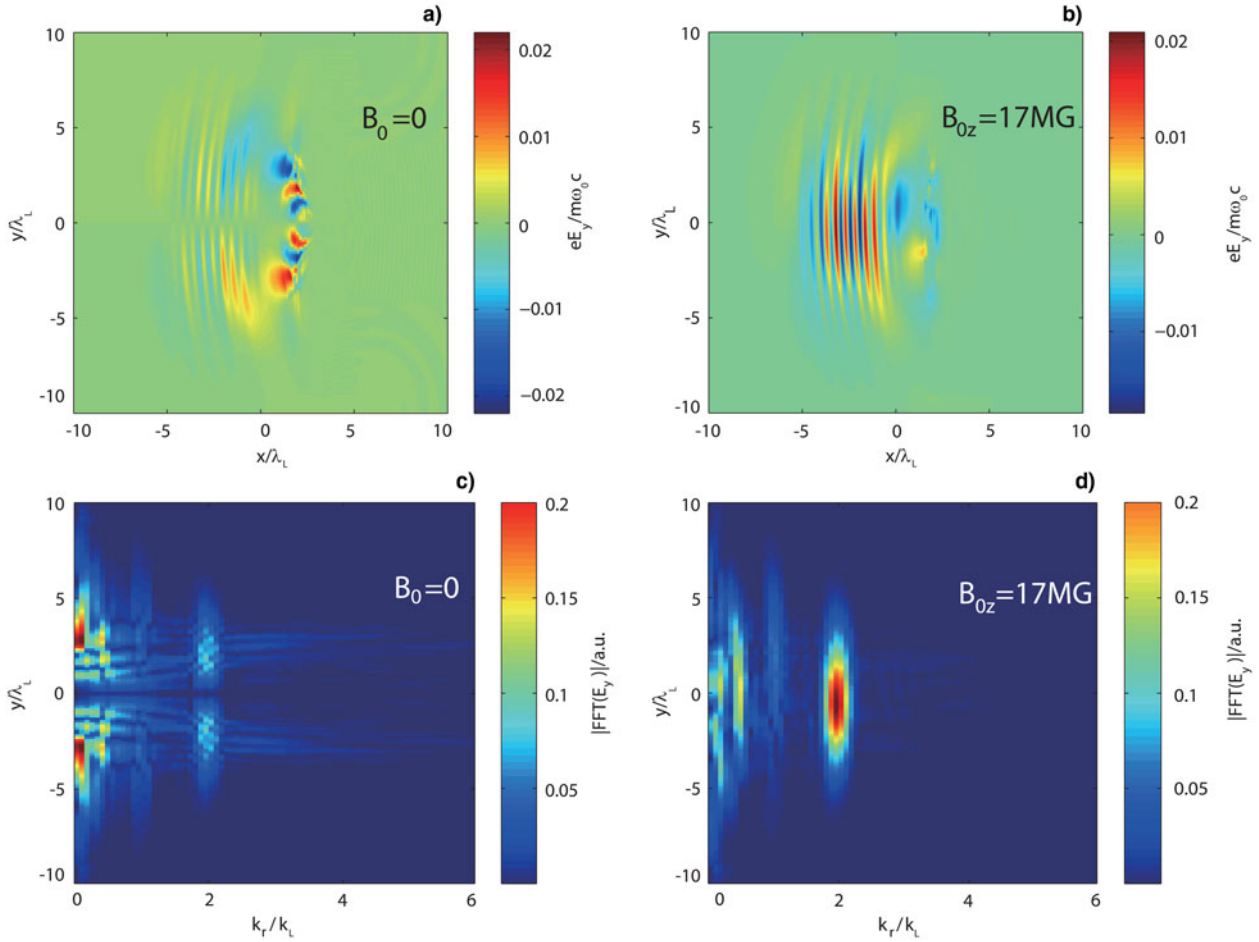


Fig. 5. Results of 3D PIC simulations. The electric field E_y of the horizontal section at $z = 0$ in the magnetic field $B_{0z} = 0$ (a) and $B_{0z} = 17$ MG (b). Plots (c) and (d) show the wave vector spectra |FFT(E_y)| for the fields given in (a) and (b), respectively. The laser focal spot size is $2\lambda_L$.

Figure 2c. Note that there is a low-frequency current component near $x/\lambda_L \sim -1$ in Figure 3a, which can be attributed to the zero-frequency component of the laser ponderomotive force and the charge separation fields at the front surface. The latter can drive longitudinal motion of electrons, which, when bended by B_{0z}, leads to low-frequency transverse currents j_y finally. The electric current component j_z shown in Figure 3b is dominated by oscillations at ω_0, even though it contains odd harmonic components. Also note that the amplitude of j_z is an order of magnitude higher than the amplitude of j_y. With the presence of magnetic field $B_{0y} = 1$ MG, there is simply $j_y = 0$. The electric current component j_z shown in Figure 3c is a kind of superposition of Figure 3a and b and is dominated by the oscillation at ω_0 as expected.

Next we look into the dependence of this magnetic field induced even harmonic generation on the magnetic field strength and plasma density scale length. Figure 4a shows a comparison of spectra for s- and p-polarized reflected light. At the magnetic field strength of 17 MG, the second harmonic due to B_{0y} is much weaker than that due to B_{0z}. However, with the increase of the magnetic field strength, it changes. As shown in Figure 4b, in a certain range (<160 MG), the spectral intensity of the second harmonic E_y depends linearly on the external magnetic field B_{0z}. It reaches the maximum at $B_{0z} = 160$ MG and weakens with stronger magnetic field. On the other hand, when applied with B_{0y}, there are several peaks in the second harmonic E_z as shown by the red circles in Figure 4b. This may be attributed to the much complicated coupling of cyclotron motion with both the longitudinal and transverse oscillations shown in Figure 1b. The almost linear scaling of the second harmonic E_y with the magnetic field B_{0z} can be used to measure the magnetic field by detecting the emission of the second harmonics or higher even harmonics. A drive pulse can be used to generate the magnetic field near the critical density region and a probe pulse can be used to measure the field (Kahaly *et al.*, 2009). By changing the focusing positions and delay of the probe pulse, the distribution and temporal evolution of the magnetic field can be measured.

So far we have fixed the preplasma scale length to be $L = 0.2\ \lambda_L$. The coupling efficiency also depends on the L employed. Figure 4c shows the correlation for the magnetic field strengths in both transverse directions with $B_{0z} = 17$ MG (blue) and $B_{0y} = 17$ MG (red). The preplasma scale of the target plays a crucial role in the surface oscillations. With the

https://doi.org/10.1017/S0263034616000446 Published online by Cambridge University Press

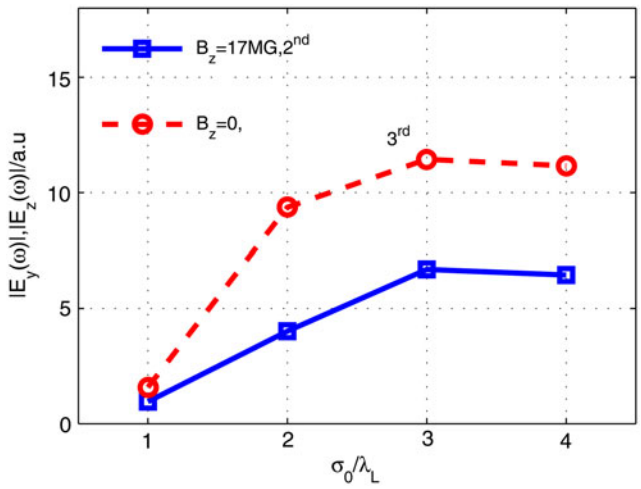


Fig. 6. Scaling of spectral intensity of the second harmonic |FFT(E_y)| (for $B_{0z} = 17$ MG) and third harmonic |FFT(E_z)| (for $B_{0z} = 0$) with the laser focal spot size obtained in 2D simulations. The electron density is steep at the surface.

parallel magnetic field B_{0z}, the even harmonic intensity increases with the density scale length L when $L < 0.2\ \lambda_L$ and then decrease with the further increase of L. This is similar to the odd harmonics produced without the effect of magnetic field (Dollar *et al.*, 2013). With the perpendicular magnetic field B_{0y}, longer preplasma with $L > 0.2\ \lambda_L$ can produce even harmonics more efficiently. This suggests that the perpendicular magnetic field leads to higher coupling at long density scale length.

3.2. Multi-dimensional effects

We also run 3D PIC simulations to check possible multi-dimensional effects on this process. The simulation box is set to be $20 \times 20 \times 20\ \lambda_L^3$ in the $x \times y \times z$-directions, with $64 \times 8 \times 8$ cells per wavelength. The plasma occupies a volume of $2 \times 18 \times 18\ \lambda_L^3$ with a sharp density front. An incident laser with a Gaussian transverse profile $a = a_0 \exp(-r^2/\sigma_0^2)$ is sent to the target from left, where $\sigma_0 = 2\ \lambda_L$is the focal spot radius at waist. The other laser parameters are the same as in the 1D simulation with the laser field polarized along the z-direction. Despite much lower spatial resolutions compared with 1D simulation, they are fine enough to resolve the second harmonics.

A pair of comparison simulations are conducted, either with or without external magnetic field B_{0z}. Figure 5 shows the p-polarized reflected fields for each case and their corresponding Fourier spectra in the k–y space. It is seen that second-harmonic generation occurs for both cases. For $B_{0z} = 0$, the harmonic is distributed in an annular pattern with a large divergence. This hollow harmonic is actually radial polarized and is probably caused by the transverse gradient of the incident laser pulse and plasma density as demonstrated in by Gizzi *et al.* (1996). While for the case of $B_{0z} = 17$ MG, the even harmonics generally share the same Gaussian transverse profile as the drive pulse. This magnetic field induced even harmonic is much higher than that produced due to the transverse gradients of the incident laser pulse.

Laser spot size is a crucial parameter for routinely monitoring high-intensity performance (Dromey *et al.*, 2009). If the laser has a large spot size, the situation is similar to 1D simulation. When the laser spot size is smaller, multi-dimensional effects such as hole boring will play a significant role and results in decrease of even-order harmonics. To show this, we carry out 2D simulations, with similar laser and plasma parameters as in 3D simulations. The spectral intensity of the second harmonics with $B_{0z} = 17$ MG is shown to increase with the laser focal spot size, and reaches saturation at $\sigma_0 = 3\ \lambda_L$. Similar results are found with the third harmonics with $B_{0z} = 0$, as shown in Figure 6. With a small laser spot size, the oscillating mirror is not a perfect planar mirror as usually found in 1D simulation, due to hole-boring effect. The reflected pulse also experiences diffraction spreading transversely, leading to decaying of the harmonic radiation quickly with the increase of distance away from the target surface. The second harmonic generated with $B_{0z} = 0$ is distributed more diversely with increasing σ_0, with the amplitude and spectral intensity increasing at first and reaching saturation at $\sigma_0 = 3\ \lambda_L$, beyond which it decreases.

4. CONCLUSION

In conclusion, it is shown that external transverse magnetic field can change the parity of harmonics generated from laser-irradiated solid surface by modifying the coupling of the transverse and longitudinal oscillations of electrons at the solid surface. In particular, with even harmonics can be produced with different polarization from the driving laser pulse. The coupling of the electron cyclotron motion and the longitudinal oscillations at the second harmonic of the driving laser is responsible for the even harmonics generation. The results are confirmed by PIC simulations. The spectral intensity of the second harmonics depends linearly on the magnitude of the magnetic field parallel to the laser electric field, providing a way to measure the strong self-generated magnetic field during the laser–plasma interaction. The dependence of the second harmonic on the preplasma scale length is shown to increase with longer preplasma scale, in which may also be useful to evaluate the preplasma scale length. Finally, both the magnetic field-induced second harmonic and normal third harmonic tend to increase with the laser spot size. When the latter is larger than $3\lambda_L$, the radiation fields become saturated. Additional even harmonic component generated due the transverse gradient of the incident laser pulse is found, which has radial polarization and emits with a conical distribution and is therefore distinctly different from the even harmonics induced by the magnetic field.

ACKNOWLEDGEMENTS

Z.M.S. would like to acknowledge the OSIRIS Consortium, consisting of UCLA and IST (Lisbon, Portugal) for the use of OSIRIS and

https://doi.org/10.1017/S0263034616000446 Published online by Cambridge University Press

the visXD framework. This work is supported by the National Science Foundation of China (grant numbers 11374210 and 11421064), a MOST international collaboration project (grant number 2014DFG02330), and a Leverhulme Trust Research Grant. Simulations were performed on the Π supercomputer at Shanghai Jiao Tong University and on the Magic Cube II supercomputer of Shanghai High Performance Computing Center. F.Y.L. and Z.M.S. acknowledge access to the ARCHER computing service through the Plasma HEC Consortium EPSRC grant number EP/L000237/1.

REFERENCES

An der Brügge, D., Kumar, N., Pukhov, A. & Rödel, C. (2012). Influence of surface waves on plasma high-order harmonic generation. *Phys. Rev. Lett.* **108**, 125002.

Bulanov, S.V., Naumova, N.M. & Pegoraro, F. (1994). Interaction of an ultrashort, relativistically strong laser pulse with an overdense plasma. *Phys. Plasmas* **1**, 745–757.

Dollar, F., Cummings, P., Chvykov, V., Willingale, L., Vargas, M., Yanovsky, V., Zulick, C., Maksimchuk, A., Thomas, A. & Krushelnick, K. (2013). Scaling high-order harmonic generation from laser–solid interactions to ultrahigh intensity. *Phys. Rev. Lett.* **110**, 175002.

Dromey, B., Bellei, C., Carroll, D.C., Clarke, R.J., Green, J.S., Kar, S., Kneip, S., Markey, K., Nagel, S.R., Willingale, L., McKenna, P., Neely, D., Najmudin, Z., Krushelnick, K., Norreys, P.A. & Zepf, M. (2009). Third harmonic order imaging as a focal spot diagnostic for high intensity laser–solid interactions. *Laser Part. Beams* **27**, 243–248.

Földes, I., Kocsis, G., Racz, E., Szatmari, S. & Veres, G. (2003). Generation of high harmonics in laser plasmas. *Laser Part. Beams* **21**, 517–521.

Fonseca, R.A., Silva, L.O., Tsung, F.S., Decyk, V.K., Lu, W., Ren, C., Mori, W.B., Deng, S., Lee, S., Katsouleas, T. & Adam, J.C. (2002). OSIRIS: a three-dimensional, fully relativistic particle in cell code for modeling plasma based accelerators. In *International Conference on Computational Science*, pp. 342–351. Berlin, Heidelberg: Springer.

Ghorbanalilu, M. (2012). Second and third harmonics generation in the interaction of strongly magnetized dense plasma with an intense laser beam. *Laser Part. Beams* **30**, 291–298.

Gizzi, L., Giulietti, D., Giulietti, A., Audebert, P., Bastiani, S., Geindre, J.-P. & Mysyrowicz, A. (1996). Simultaneous measurements of hard × rays and second-harmonic emission in fs laser–target interactions. *Phys. Rev. Lett.* **76**, 2278.

Kahaly, S., Monchocé, S., Vincenti, H., Dzelzainis, T., Dromey, B., Zepf, M., Martin, P. & Quéré, F. (2013). Direct observation of density-gradient effects in harmonic generation from plasma mirrors. *Phys. Rev. Lett.* **110**, 175001.

Kahaly, S., Mondal, S., Kumar, G.R., Sengupta, S., Das, A. & Kaw, P. (2009). Polarimetric detection of laser induced ultrashort magnetic pulses in overdense plasma. *Phys. Plasmas* **16**, 043114.

Lichters, R., Meyer-ter Vehn, J. & Pukhov, A. (1996). Short-pulse laser harmonics from oscillating plasma surfaces driven at relativistic intensity. *Phys. Plasmas* **3**, 3425–3437.

Ma, T., Sawada, H., Patel, P.K., Chen, C.D., Divol, L., Higginson, D.P., Kemp, A.J., Key, M.H., Larson, D.J., Le Pape, S., Link, A., MacPhee, A.G., McLean, H.S., Ping, Y., Stephens, R.B., Wilks, S.C. & Beg, F.N. (2012). Hot electron temperature and coupling efficiency scaling with prepulse for cone-guided fast ignition. *Phys. Rev. Lett.* **108**, 115004.

MacPhee, A.G., Divol, L., Kemp, A.J., Akli, K.U., Beg, F.N., Chen, C.D., Chen, H., Hey, D.S., Fedosejevs, R.J., Freeman, R.R., Henesian, M., Key, M.H., Le Pape, S., Link, A., Ma, T., Mackinnon, A.J., Ovchinnikov, V.M., Patel, P.K., Phillips, T.W., Stephens, R.B., Tabak, M., Town, R., Tsui, Y.Y., Van Woerkom, L.D., Wei, M.S. & Wilks, S.C. (2010). Limitation on prepulse level for cone-guided fast-ignition inertial confinement fusion. *Phys. Rev. Lett.* **104**, 055002.

Mairesse, Y., De Bohan, A., Frasinski, L.J., Merdji, H., Dinu, L.C., Monchicourt, P., Breger, P., Kovačev, M., Taeb, R., Carré, B., Muller, H.G., Agostini, P. & Salières, P. (2003). Attosecond synchronization of high-harmonic soft x-rays. *Science* **302**(5650), 1540–1543.

Mason, R. & Tabak, M. (1998). Magnetic field generation in high-intensity-laser–matter interactions. *Phys. Rev. Lett.* **80**, 524.

Ozaki, T., Elouga Bom, L., Ganeev, R., Kieffer, J.-C., Suzuki, M. & Kuroda, H. (2007). Intense harmonic generation from silver ablation. *Laser Part. Beams* **25**, 321–325.

Quéré, F., Thaury, C., Monot, P., Dobosz, S., Martin, P., Geindre, J.-P. & Audebert, P. (2006). Coherent wake emission of high-order harmonics from overdense plasmas. *Phys. Rev. Lett.* **96**, 125004.

Sheng, Z.-M., Mima, K., Zhang, J. & Sanuki, H. (2005). Emission of electromagnetic pulses from laser wakefields through linear mode conversion. *Phys. Rev. Lett.* **94**, 095003.

Stambulchik, E., Tsigutkin, K. & Maron, Y. (2007). Spectroscopic method for measuring plasma magnetic fields having arbitrary distributions of direction and amplitude. *Phys. Rev. Lett.* **98**, 225001.

Sudan, R.N. (1993). Mechanism for the generation of 10^9 g magnetic fields in the interaction of ultraintense short laser pulse with an overdense plasma target. *Phys. Rev. Lett.* **70**, 3075–3078.

Tatarakis, M., Watts, I., Beg, F.N., Clark, E.L., Dangor, A.E., Gopal, A., Haines, M.G., Norreys, P.A., Wagner, U., Wei, M.-S., Zepf, M. & Krushelnick, K. (2002). Laser technology: measuring huge magnetic fields. *Nature* **415**(6869), 280–280.

Tsakiris, G.D., Eidmann, K., Meyer-ter Vehn, J. & Krausz, F. (2006). Route to intense single attosecond pulses. *New J. Phys.* **8**, 19.

Weng, S., Murakami, M. & Sheng, Z. (2015). Reducing ion energy spread in hole-boring radiation pressure acceleration by using two-ion-species targets. *Laser Part. Beams* **33**, 103–107.

Yeung, M., Bierbach, J., Eckner, E., Rykovanov, S., Kuschel, S., Sävert, A., Förster, M., Rödel, C., Paulus, G.G., Cousens, S., Coughlan, M., Dromey, B. & Zepf, M. (2015). Noncollinear polarization gating of attosecond pulse trains in the relativistic regime. *Phys. Rev. Lett.* **115**, 193903.

Zepf, M., Castro-Colin, M., Chambers, D., Preston, S.G., Wark, J.S., Zhang, J., Danson, C.N., Neely, D., Norreys, P., Dangor, A.E., Dyson, A., Lee, P., Fews, A.P., Gibbon, P., Moustaizis, S. & Key, M.H. (1996). Measurements of the hole boring velocity from Doppler shifted harmonic emission from solid targets. *Phys. Plasmas* **3**, 3242–3244.

Zheng, J., Tanaka, K., Sentoku, Y., Offenberger, A., Kitagawa, Y., Kodama, R., Kurahashi, T., Mima, K. & Yamanaka, T. (2002). Harmonic emission with cyclotron satellite structure due to strong magnetic fields produced by ultra-intense laser–-plasma interaction. *Phys. Plasmas* **9**, 3193–3196.

https://doi.org/10.1017/S0263034616000446 Published online by Cambridge University Press